



RESEARCH LETTER

10.1002/2016GL068337

Key Points:

- We measure key subglacial channel physical parameters from the analysis of seismic ground motion
- Water input changes are accommodated by pressure gradient changes at short time scales and by channel size changes at longer time scales
- Increases in subglacial channel pressure gradient correlate with increases in glacier velocity and sediment transport

Supporting Information:

- Supporting Information S1

Correspondence to:

F. Gimbert,
flo.gimbert1754@gmail.com

Citation:

Gimbert, F., V. C. Tsai, J. M. Amundson, T. C. Bartholomew, and J. I. Walter (2016), Subseasonal changes observed in subglacial channel pressure, size, and sediment transport, *Geophys. Res. Lett.*, 43, doi:10.1002/2016GL068337.

Received 8 DEC 2015

Accepted 5 APR 2016

Accepted article online 7 APR 2016

Subseasonal changes observed in subglacial channel pressure, size, and sediment transport

Florent Gimbert^{1,2,3}, Victor C. Tsai^{1,2}, Jason M. Amundson⁴, Timothy C. Bartholomew⁵, and Jacob I. Walter⁵

¹Seismological Laboratory, California Institute of Technology, Pasadena, California, USA, ²Division of Geological and Planetary Sciences, California Institute of Technology, Pasadena, California, USA, ³Now at GFZ Deutsches GeoForschungszentrum, Potsdam, Germany, ⁴Department of Natural Sciences, University of Alaska Southeast, Juneau, Alaska, USA, ⁵Institute for Geophysics, University of Texas at Austin, Austin, Texas, USA

Abstract Water that pressurizes the base of glaciers and ice sheets enhances glacier velocities and modulates glacial erosion. Predicting ice flow and erosion therefore requires knowledge of subglacial channel evolution, which remains observationally limited. Here we demonstrate that detailed analysis of seismic ground motion caused by subglacial water flow at Mendenhall Glacier (Alaska) allows for continuous measurement of daily to subseasonal changes in basal water pressure gradient, channel size, and sediment transport. We observe intermittent subglacial water pressure gradient changes during the melt season, at odds with common assumptions of slowly varying, low-pressure channels. These observations indicate that changes in channel size do not keep pace with changes in discharge. This behavior strongly affects glacier dynamics and subglacial channel erosion at Mendenhall Glacier, where episodic periods of high water pressure gradients enhance glacier surface velocity and channel sediment transport by up to 30% and 50%, respectively. We expect the application of this framework to future seismic observations acquired at glaciers worldwide to improve our understanding of subglacial processes.

1. Introduction

Subglacial channel dynamics plays a primary role in controlling glacier sliding and thereby influences glacier and ice sheet mass balance and landscape evolution. For example, drag at the ice-bed interface depends on effective normal stress such that high basal water pressure promotes increased basal sliding velocities [Iken and Bindshadler, 1986; Bartholomew et al., 2010; Andrews et al., 2014]. Rapid sliding, in turn, increases abrasion and potentially leads to net enhancement of glacial erosion [Hallet, 1979; Alley et al., 1997; Herman et al., 2015]. Predicting glacier sliding, however, remains challenging as it requires knowledge of the response of subglacial channels to changes in water input. Pressurization of distributed (e.g., linked cavity) systems with inefficient drainage is thought to cause enhanced glacier sliding [Liboutry, 1968; Iken, 1981; Kamb et al., 1985; Bartholomew et al., 2008], while well-connected (e.g., channelized) systems forming during the melt season are thought to seasonally prevent sustained overpressurization [Röthlisberger, 1972; Schoof, 2010] and thus reduce sliding [Mair et al., 2002]. These conceptual models, though, are difficult to test since flow tracers [e.g., Stenborg, 1969; Hooke et al., 1988; Kohler, 1995], borehole pressure sensors [e.g., Mathews, 1964; Iken and Bindshadler, 1986; Hubbard et al., 1995; Murray and Clarke, 1995; Andrews et al., 2014; Schoof et al., 2014], and active seismic, resistivity, and radar imaging measurements [e.g., Vincent et al., 2012; Legchenko et al., 2014] only provide temporally and spatially limited observations. There are presently no observational methods that enable simultaneous constraints on channel geometry and water pressure.

Here we overcome these observational difficulties by using ambient ground motion (also “noise” or “tremor”), recorded with seismometers to continuously and remotely monitor the temporal evolution of subglacial water pressure gradients, channel size, and bedload sediment transport. As opposed to conventional instrumentation, seismometers offer the substantial advantage of being easy to deploy, maintain, and capable of providing continuous measurements of subglacial channel properties averaged over the catchment scale (~1 km, see Tsai et al. [2012] and Gimbert et al. [2014]), i.e., over the representative scale at which numerical models are evaluated [Flowers and Clarke, 2002; Schoof, 2010; Werder et al., 2013].

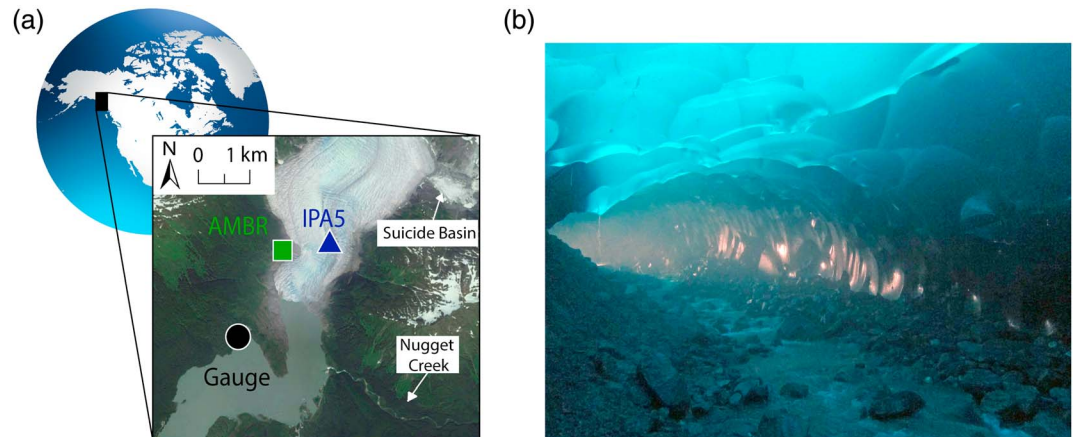


Figure 1. (a) Map of the Mendenhall Glacier (Alaska) field site and (b) photograph of a subglacial conduit beneath the Mendenhall Glacier terminus after the end of the melt season. The conduit is several meters in diameter and is located on the western margin of the glacier between seismic station AMBR (green square) and Mendenhall Lake. Additional instruments used in this study are the GPS station IPA5 (blue triangle) and the lake gauge station (black circle). Suicide Basin was the source of the outburst flood that initiated on 3 July. Nugget Creek is the other main source of inflow into Mendenhall Lake.

2. Data and Theory

We use recent observations of high frequency (1–20 Hz) seismic noise caused by subglacial water flow through channels at Mendenhall Glacier, Alaska [see *Bartholomaeus et al.*, 2015]. Seismic noise was recorded by station AMBR installed on a rock outcrop about 50–100 m west of the glacier edge and 2 km upstream of the lacustrine-calving glacier terminus (Figure 1a). The glacier is about 1 km wide near the seismic station, such that all subglacial channels may contribute to the observed seismic noise, with closer channels contributing more than distant ones due to seismic wave attenuation [*Gimbert et al.*, 2014]. A GPS station, IPA5, was deployed on the glacier surface and was located within the domain of sensitivity of the seismic station; glacier motion recorded by the GPS receiver was therefore representative of the region for which channel-induced noise was recorded. Variations in water discharge Q from Mendenhall Glacier were obtained by applying mass conservation to the proglacial lake such that $Q = Q_{\text{out}} + \Omega dh/dt$ where lake discharge Q_{out} and lake stage h were measured by the U.S. Geological Survey and Ω is lake area [*Bartholomaeus et al.*, 2015]. Our indirect measurements of variations in Q thus rely on lake inflow from sources (mainly Nugget Creek, see Figure 1) being small or covarying with that of Mendenhall Glacier, which we verified from direct discharge measurements over the period 2000–2004 and from melt and precipitation calculations (supporting information).

Seismic noise theory originally developed for fluvial applications [*Gimbert et al.*, 2014] indicates that seismic power P_w at low frequencies (typically 2 to 5 Hz, see blue line of Figure 2a) is primarily caused by turbulent water flow noise, whereas seismic power P_b at higher frequencies (typically 10 to 20 Hz, see red line of Figure 2a) is primarily caused by impact events from bedload sediment transport, i.e., from rolling or saltating particles (see also the observations of *Burtin et al.* [2011] and *Schmandt et al.* [2013]). The power of turbulent flow-induced noise in rivers is predicted to scale as

$$P_w \propto \zeta W u_*^{14/3} \quad (1)$$

where u_* is shear velocity, W is river width, and $\zeta = \zeta\left(\frac{H}{k_s}\right)$ is a function that expresses the decrease of bed-flow turbulence intensity and average flow velocity with rougher flows, where H is flow depth and k_s is wall roughness size [*Gimbert et al.*, 2014]. ζ thus varies significantly with flow depth for $H \sim k_s$ but becomes nearly constant for $H \gg k_s$ (supporting information).

We apply the framework to subglacial channels by making three assumptions. First, we assume uniform pressure fluctuations along the walls of the channels as a result of similar wall shear stress and roughness

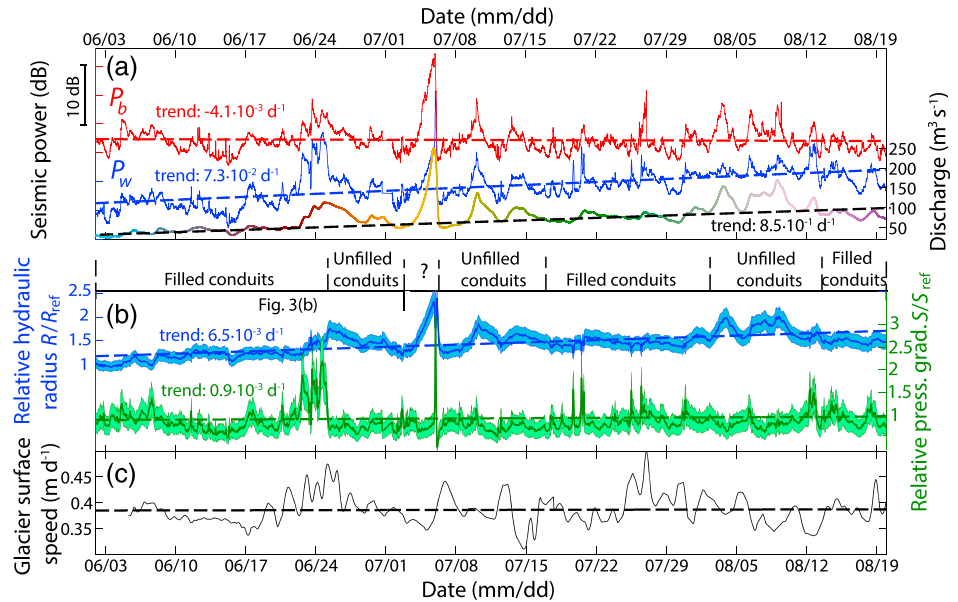


Figure 2. Time series of physical quantities measured during summer 2012 at Mendenhall Glacier. Continuous lines show measurements, and dashed lines show best fitting linear trends. (a) Seismic power at station AMBR (Figure 1) in the bedload (P_b , red line) and water (P_w , blue line) frequency ranges, and subglacial discharge Q as inferred from lake mass balance analysis (colors correspond to Figure 3). (b) Relative channel hydraulic radius (blue line) and water pressure (green line) as inferred from the combined analysis of P_w and Q (see equations (4.1) and (4.2)). The first day of the recorded time period (2 June) has been chosen as reference. Light blue and light green shaded areas show uncertainties on R and S (supporting information). Uncertainties are mainly due to channel shape uncertainty for R and to relative flow roughness uncertainty for S . Time periods of unfilled versus filled conduits are interpreted on the basis of whether pressure is relatively low and P_w scales as $Q^{5/4}$ or pressure is relatively high and P_w scales as $Q^{14/3}$ (see also Figure 3). (c) Glacier surface velocity from GPS station IPAS (Figure 1).

([Gulley *et al.*, 2014], see also Figure 1b), regardless of whether the walls are composed of ice, sediment, or bedrock. We thus replace river width W in equation (1) by the wetted perimeter Γ . We note that Γ should scale with channel width even if seismic radiation into the ice significantly differs from that into the ground. Second, we neglect variations in ζ since flow depth H (typically meter size) is expected to be much larger than k_s (typically centimeter to decimeter size, see Figure 1b) in the efficient channels predicted by theory to dominate the production of seismic noise (see below). Thus, ζ is expected to show little variation (see supporting information for uncertainty estimates due to neglecting ζ). Third, we assume that subglacial channel flow is steady and uniform when averaged over the largest turbulent spatial (of order several flow depths) and temporal (of order several seconds) scales (which we verify *a posteriori*) such that shear velocity can be expressed as $u_* = \sqrt{gRS}$ where g is gravitational acceleration, $R = \frac{A}{\Gamma}$ is hydraulic radius, and A is cross-sectional area; $S = -\frac{1}{\rho g} \frac{\partial p}{\partial x} + \tan \theta$ is hydraulic pressure gradient, where θ is channel bed slope, ρ is water density, p is water pressure, and x is distance in the flow direction (positive downstream). Under these assumptions, P_w as defined in equation (1) becomes

$$P_w \propto \Gamma R^{7/3} S^{7/3}. \tag{2}$$

This expression for P_w holds for multiple channels (in which case Γ , R , and S are weighted average values) as long as the total number of channels and their respective positions do not significantly vary with time. Order of magnitude model estimates of the observed seismic noise absolute power (-180 to -150 dB [Gimbert *et al.*, 2014; see also Bartholomaus *et al.*, 2015]) suggest that seismic noise is caused by subglacial flow velocities on the order of ~ 1 m/s. Seismic noise is thus likely caused by the relatively high flow velocities (of order 1 m/s) within well-connected efficient drainage channels [Kohler, 1995; Mair *et al.*, 2002] and is unlikely to be due to much slower flows (of order 1 cm/s) within orifices and cavities of an inefficient drainage network [Brugman, 1986; Kamb, 1987].

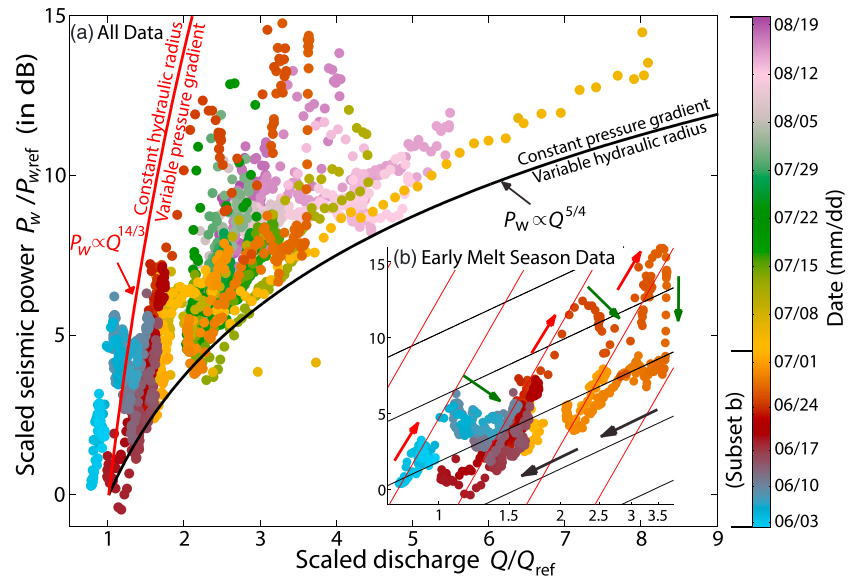


Figure 3. Predicted and observed scaled seismic power versus scaled water discharge for (a) all 1 h binned measurements (x axis scale is linear) and (b) during the early melt season (x axis scale is logarithmic). The color scale for all observations is consistent and varies with time over the melt season. Reference power $P_{w,ref}$ and discharge Q_{ref} are taken near minimum power and minimum discharge. Lines show model predictions for constant channel pressure gradient and varying hydraulic radii (in black), and constant hydraulic radii and varying pressure gradient (in red). Arrows in Figure 3b highlight characteristic behaviors of channel pressurization (red arrows) and depressurization (green arrows), as well as channel hydraulic radii decrease at constant, low-pressure gradient (black arrows).

To evaluate how seismic power P_w defined as a function of R and S in equation (2) relates to flow discharge $Q = AU$, where U is average velocity, we substitute U from the Manning-Strickler formulation as $U = \frac{R^{2/3}S^{1/2}}{n'}$ (n' is Manning's coefficient, see Manning [1891] and Strickler [1923, 1981]) and arrive at

$$Q \propto AR^{2/3}S^{1/2}. \tag{3}$$

Writing Γ and A as a function of R as $\Gamma = \beta R$ and $A = \beta R^2$, where β is a function of conduit shape and fullness (supporting information), substituting these expressions into equation (2) for P_w and equation (3) for Q , and writing P_w as a function of R and Q or S and Q , we obtain

$$P_w \propto \beta^{-11/3}R^{-82/9}Q^{14/3} \tag{4.1}$$

$$P_w \propto \beta^{-1/4}S^{41/24}Q^{5/4}. \tag{4.2}$$

If channel geometry remains constant with discharge (β and R constant), then changes in discharge occur through changes in shear velocity (equation (1)), and equation (4.1) implies $P_w \propto Q^{14/3}$ regardless of conduit shape (e.g., circular or semicircular and elongated). On the other hand, if hydraulic pressure gradient S is constant, then equation (4.2) implies $P_w \propto \beta^{-1/4}Q^{5/4}$. Moreover, since $\beta^{-1/4}$ variations are at least an order of magnitude smaller than observed $Q^{5/4}$ variations (see supporting information), $P_w \propto Q^{5/4}$ is approximately appropriate for channels at constant pressure gradient (regardless of conduit shape and degree of fullness). Seismic power thus weakly scales with discharge for channels with constant pressure gradient and varying hydraulic radii but strongly scales with discharge for channels with constant hydraulic radii and varying pressure gradient.

3. Results and Discussion

3.1. Predicted Versus Observed Scalings

Data over the melt season at Mendenhall Glacier follow the theoretical predictions (Figure 3a), with all data points exhibiting a general trend between that of the constant pressure gradient and constant hydraulic

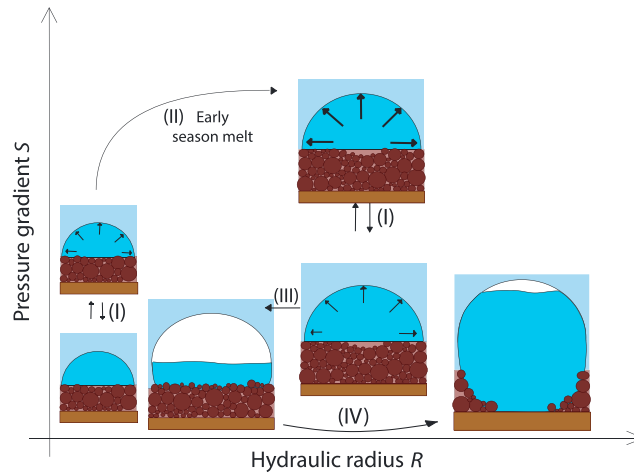


Figure 4. Schematic showing the different subglacial channel regimes inferred from seismic noise. Grains represent a sediment till layer, while the bottom light brown layer represents hard bedrock. Arrows in conduits indicate pressure gradient, with arrow lengths proportional to amplitude. Numbers are cited in the main text and refer to (I) pressure gradient changes occurring at constant hydraulic radii, (II) conduit growth through melting of ice, (III) conduits transitioning from filled to unfilled, and (IV) conduits increasing hydraulic radius through enhanced sediment transport.

radii predictions. Moreover, the inferred changes in pressure gradient show that subglacial conduits often do not adjust their hydraulic radii fast enough to accommodate discharge changes, and highly pressurized channels occur frequently, for example, during the large daily melt events occurring in the early summer season (2 June to 3 July, see Figure 3b) in response to melt discharge input (supporting information). Specifically, our analysis reveals several hours to weeklong time periods during which seismic power approximately follows the $P_w \propto Q^{14/3}$ scaling prediction for constant hydraulic radii and varying pressure gradient (e.g., Figure 3b red arrows, which occur mostly during rapidly rising discharge). Since discharge varies over these time scales, this implies that conduits must be filled and that discharge changes cause pressure gradient changes without significantly changing conduit size. At

other times, though, particularly during falling discharge, seismic power instead follows the $P_w \propto Q^{5/4}$ scaling prediction for constant pressure gradient and varying hydraulic radii (e.g., Figure 3b black arrows), implying a very different flow regime. In addition to the constant pressure gradient and constant hydraulic radii scalings, time periods of complex, intermediate behavior are also observed, for example, where P_w falls even as Q continues to rise (e.g., Figure 3b green arrows). This pattern reflects decreases in pressure gradient that initiate as the rate of input discharge (from melt and/or rain) reaches its maximum (not shown). We suggest that these decreases in pressure gradient eventually result in a new, steady state with larger channel size and lower absolute pressure. The observed relationships between P_w and Q also support the conclusion that subglacial channels are the main contributors to the recorded seismic noise. In surface streams, P_w should consistently scale with $Q^{7/5}$ (using constant Γ and $A \approx R$ in equations (2) and (3)), which is not observed.

3.2. Inferring Water Pressure Gradient and Channel Hydraulic Radius Changes

Further insight into subglacial channel evolution and its connection with glacier sliding and bedload transport can be drawn by solving for channel hydraulic pressure gradient S and hydraulic radius R in equations (4.1) and (4.2). Neglecting the weak dependence of model predictions on channel shape and fullness (supporting information), we obtain

$$S = S_{\text{ref}} \left(\frac{P_w}{P_{w,\text{ref}}} \right)^{24/41} \left(\frac{Q}{Q_{\text{ref}}} \right)^{-30/41} \tag{5}$$

$$R = R_{\text{ref}} \left(\frac{P_w}{P_{w,\text{ref}}} \right)^{-9/82} \left(\frac{Q}{Q_{\text{ref}}} \right)^{21/41}$$

where ref denotes an arbitrary reference state. Consistent with subglacial drainage of increasing efficiency over the course of the summer [Kohler, 1995; Mair et al., 2002; Bartholomew et al., 2010], R increases (by a factor of 1.4) while S exhibits a negligible trend over the melt season (Figure 2b). However, on time scales shorter than a week, S often varies much more than R , again showing that conduits do not adjust their size fast enough to accommodate changes in discharge (see also Figure 4(I)). Thus, channel size is often not in equilibrium with discharge, and the common expectation that channel pressure decreases as discharge increases for well-connected drainage systems [Röthlisberger, 1972] does not hold over time scales up to several days. Röthlisberger's prediction of $S \propto Q^2$ for constant channel radius (see equation (10) of Röthlisberger [1972]), however, is in agreement with our observations, as during the large melt events of 22–27 June when diurnal

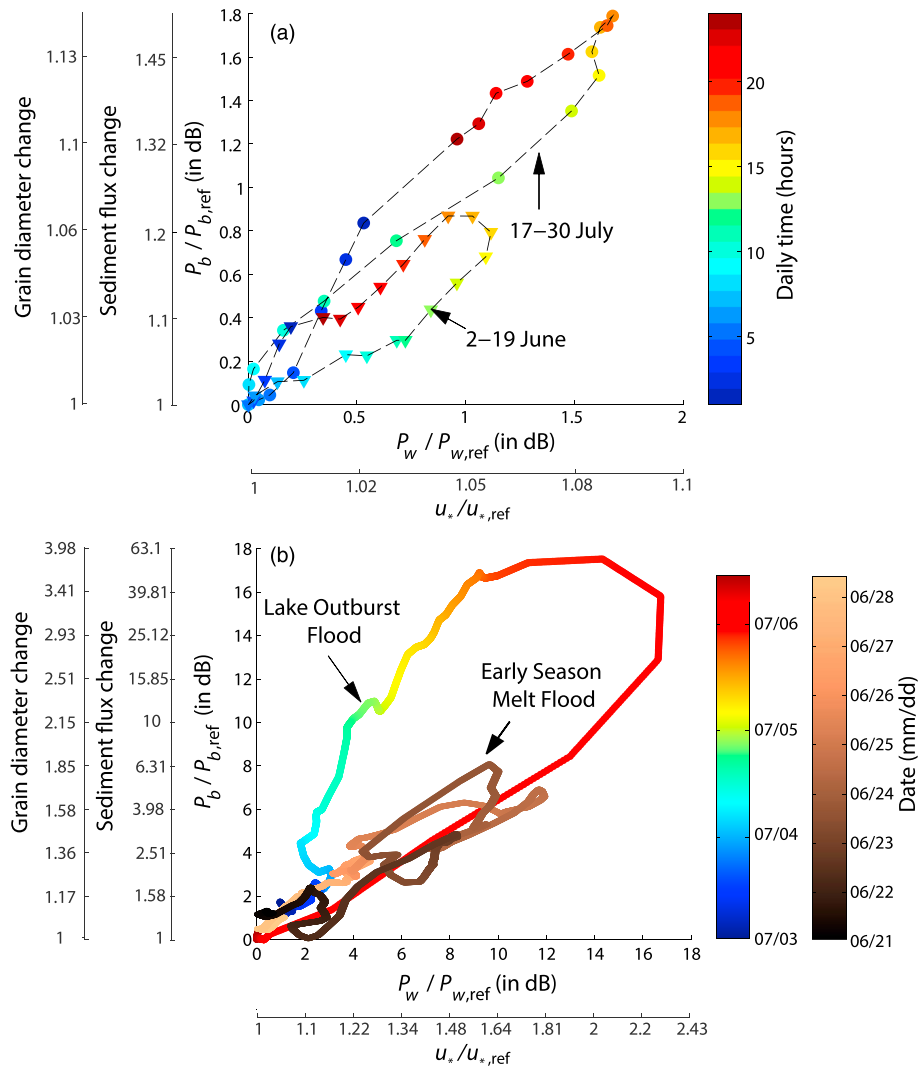


Figure 5. Scaled bedload-induced seismic power P_b as a function of scaled water flow-induced seismic power P_w for various time periods. (a) Daily values of P_b and P_w averaged by hour over two approximately 2 weeklong time periods when conduits are filled and diurnal pressure gradient fluctuations are large. (b) Changes in P_b versus P_w during the largest melt event of 21–29 June and during the lake outburst flood of 3–7 July. Changes in P_w and P_b have also been converted into changes in shear velocity u_* ($P_w \propto u_*^{14/3}$, see equation (1) and *Gimbert et al.* [2014]) and changes in sediment transport flux q_b and transported grain diameter D ($P_b \propto q_b D^3$, see *Tsai et al.* [2012]).

changes in Q by a factor of 1.5 are associated with diurnal changes in S by about a factor of $(1.5)^2 \approx 2$, while R remains nearly constant. In addition, as might be expected, times of high-pressure gradient (and thus presumably also high absolute pressure) in channels occur at times of high glacier surface speed [*Andrews et al.*, 2014]. For example, surface speed increases by up to 30% from 17 June to 25 June (Figure 2c), when absolute pressures are inferred to be highest. These maximum values of absolute water pressure (estimated by spatially integrating observed pressure gradients) are on the order of overburden pressure, consistent with episodic daily to weekly fluctuations in pressure gradient (indicative of water pressure fluctuations) being correlated with glacier surface speed during the early melt season (correlation coefficient is 0.61 from 3 June to 25 June, see supporting information). Though significant, this correlation is not as high as that observed in certain previous studies [*Iken and Bindshadler*, 1986; *Andrews et al.*, 2014]. This may be due to seismic observations being most sensitive to pressure gradient changes in regions of fast water flow, which likely only partly reflect pressure changes in the poorly drained regions adjacent to subglacial conduits that are expected to exert the strongest control on sliding [*Mair et al.*, 2002; *Andrews et al.*, 2014]. Uncertainties in our seismically constrained pressure inferences may also contribute to the relatively poor correlation.

In contrast to time periods with rapid variations in S , we observe that at other times R varies much more than S (see 26 June to 16 July and 1–20 August in Figure 2b), with large hydraulic radii changes (by 10 to 100%) occurring over short, multiday time scales and at relatively low, stable pressure gradients. We suggest that channels are unfilled during most of these periods, in which case water depth and thus channel radius evolve freely. Unfilled channels are thought to occur for mountain glaciers with relatively thin (100 m thick) ice on steep bedrock [Lliboutry, 1983; Hooke, 1984]. Thus, unfilled channels could occur near the terminus of lake terminating Mendenhall Glacier where thin ice (~100–300 m) and subglacial channels draining from higher elevations are expected (supporting information and Motyka *et al.* [2003]). The unexpected variations of S during time periods when conduits are interpreted to be unfilled (as labeled in Figure 2b) may be an artifact of neglecting changes in ζ from apparent roughness changes in our model predictions (see equation (1) and supporting information).

3.3. Links With Sediment Transport in Channels

High pressure gradient situations have important implications for the contribution of subglacial channels to glacial erosion and sediment transport budgets. We estimate changes in bed shear velocity u_* from changes in P_w (using $P_w \propto u_*^{14/3}$, see equation (1) and Gimbert *et al.* [2014]) as well as changes in sediment transport flux q_b and transported grain diameter D from changes in P_b (using $P_b \propto q_b D^3$, see Tsai *et al.* [2012]). As described above, small diurnal changes in discharge are accommodated primarily by pressure gradient variations rather than hydraulic radius changes (see corresponding periods in Figure 2b). During these times, sediment transport and transported grain size could be significantly increased [Alley *et al.*, 1997]. For example, during the diurnal pressure gradient fluctuations of periods 2–19 June and 17–30 July (Figure 2b), shear velocities increase by about 5–7%, which may enhance sediment transport flux by a factor of 1.25 to 1.5 (i.e., an increase of 25%–50%) or transported grain diameter by a factor of 1.1 (i.e., an increase of 10%) from low to high hydraulic gradient times (Figure 5a). These high pressure gradients ensure that subglacial sediments are efficiently carried downstream by subglacial channels during the melt season. This is confirmed by our bedload proxy observations, since increasing discharge over the melt season is not accompanied by increasing bedload noise, which instead gradually decreases (Figure 2a, see also Riihimaki *et al.* [2005]). This implies that channel bedload transport may be seasonally limited by sediment production from glacier abrasion or plucking rather than by channel transport capacity.

Limited sediment supply is not only observed at the seasonal time scale but also during an outburst flood associated with the drainage of an ice marginal lake in Suicide Basin (see Figure 1a) from 3 to 7 July. Unlike during the largest melt event of 22–28 June, the outburst flood shows a pronounced (10 dB) sediment transport hysteresis versus shear velocity (Figure 5b). This hysteresis is thus not restricted to a hysteresis versus water discharge [Riihimaki *et al.*, 2005] (which could be explained solely by changes in pressure gradient for similar discharges) but instead indicates that sediments are exhausted from channels over the course of the event. This process could be an efficient way in which subglacial conduits erode subglacial till and thus increase size rapidly with discharge (Figure 4(IV)). Sediment erosion would complement wall melt and allow conduits to remain unfilled and at low water pressure gradient, such as observed during this lake drainage event (Figure 2b). We note, however, that the slow, multiday increase in channel size and discharge at constant pressure gradient are also consistent with the jökulhlaup theory of Nye [1976], without requiring till erosion.

4. Conclusions

Here we have established a seismological framework that, when combined with water discharge measurements, allows for the continuous monitoring of daily to seasonal variability of subglacial channel pressure gradient, hydraulic radius, and sediment transport. While both long and short-term variations in seismic noise follow variations in discharge [Bartholomaus *et al.*, 2015], the use of our quantitative, modeling framework allows us to separate the respective contributions of pressure gradient-mediated versus hydraulic radius-mediated flow speed on the production of total seismic noise or tremor amplitude. We find that seismic power is most sensitive to discharge when the pressure gradient-mediated water flow speed drives variations in subglacial discharge. We also observe that channel pressure gradient exhibits significant hourly to multiday variability caused by changes in the rate of water input but that its longer-term mean value is stable over the period of observations. Over weekly and longer time scales, changes in discharge are instead

accommodated through changes in conduit size. These results provide fresh insight into the high-frequency evolution of subglacial conduits, while supporting the validity of prevailing, steady state conduit models [Röthlisberger, 1972] at longer time scales, over which seismic noise could be used to infer discharge in settings where it is otherwise unknown. Our results are consistent with a view that, beneath the thin, terminal ice of Mendenhall Glacier, subglacial conduits are unable to adjust their size quickly enough to accommodate the highly variable, short time scale changes in water input without significant pressurization. On the other hand, these same subglacial conduits have the ability to close slowly enough that the continuous increase in subglacial discharge throughout the melt season does not cause a significant, weekly and longer time scale increase in pressure gradient.

Using our seismological framework, we also observe, as expected, that subglacial channel dynamics strongly controls glacier sliding and subglacial sediment transport. Channel pressure gradient (and presumably also channel pressure) is correlated with glacier velocity measured from GPS and subglacial channel sediment transport measured from higher-frequency seismic noise. Both at seasonal time scales and during an outburst flood, though, we observe subglacial sediment transport hysteresis with channel bed shear stress, consistent with subglacial sediment transport being limited by sediment production from glacier erosion or sediment availability. This seismological framework thus provides unique constraints on the complex mechanical interactions between ice, water, and sediments and their role in glacier sliding and erosion. We expect the application of this framework to future seismic observations acquired at various glaciers including in Greenland and Antarctica to significantly improve our knowledge of glacier basal processes.

Acknowledgments

This study was funded by NSF grant EAR-1453263. We thank Flavien Beaud and an anonymous reviewer for thorough reviews that improved the manuscript. We also thank Michael Lamb, Olivier Gagliardini, Jean-Philippe Avouac, Gael Durand and Adrien Gilbert for fruitful discussions.

References

- Alley, R. B., K. M. Cuffey, E. B. Evenson, J. C. Strasser, D. E. Lawson, and G. J. Larson (1997), How glaciers entrain and transport basal sediment: Physical constraints, *Quat. Sci. Rev.*, *16*(9), 1017–1038, doi:10.1016/S0277-3791(97)00034-6.
- Andrews, L. C., G. A. Catania, M. J. Hoffman, J. D. Gulley, M. P. Lüthi, C. Ryser, R. L. Hawley, and T. A. Neumann (2014), Direct observations of evolving subglacial drainage beneath the Greenland Ice Sheet, *Nature*, *514*(7520), 80–83, doi:10.1038/nature13796.
- Bartholomäus, T. C., R. S. Anderson, and S. P. Anderson (2008), Response of glacier basal motion to transient water storage, *Nat. Geosci.*, *1*(1), 33–37, doi:10.1038/ngeo.2007.52.
- Bartholomäus, T. C., J. M. Amundson, J. I. Walter, S. O'Neel, M. E. West, and C. F. Larsen (2015), Subglacial discharge at tidewater glaciers revealed by seismic tremor, *Geophys. Res. Lett.*, *42*, 6391–6398, doi:10.1002/2015GL064590.
- Bartholomew, I., P. Nienow, D. Mair, A. Hubbard, M. A. King, and A. Sole (2010), Seasonal evolution of subglacial drainage and acceleration in a Greenland outlet glacier, *Nat. Geosci.*, *3*(6), 408–411, doi:10.1038/ngeo863.
- Brugman, M. M. (1986), Water flow at the base of a surging glacier, PhD thesis, Calif. Inst. of Technol.
- Burtin, A., R. Cattin, L. Bollinger, J. Vergne, P. Steer, A. Robert, N. Findling, and C. Tiberi (2011), Towards the hydrologic and bed load monitoring from high-frequency seismic noise in a braided river: The "Torrent de St Pierre", French Alps, *J. Hydrol.*, *408*(1–2), 43–53, doi:10.1016/j.jhydrol.2011.07.014.
- Flowers, G. E., and G. K. C. Clarke (2002), A multicomponent coupled model of glacier hydrology 1. Theory and synthetic examples, *J. Geophys. Res.*, *107*(B11), 2287, doi:10.1029/2001JB001122.
- Gimbert, F., V. C. Tsai, and M. P. Lamb (2014), A physical model for seismic noise generation by turbulent flow in rivers, *J. Geophys. Res. Earth Surf.*, *119*, 2209–2238, doi:10.1002/2014JF003201.
- Gulley, J. D., P. D. Spellman, M. D. Covington, J. B. Martin, D. I. Benn, and G. Catania (2014), Large values of hydraulic roughness in subglacial conduits during conduit enlargement: Implications for modeling conduit evolution, *Earth Surf. Processes Landforms*, *39*(3), 296–310, doi:10.1002/esp.3447.
- Hallet, B. (1979), A theoretical model of glacial abrasion, *J. Glaciol.*, *23*, 39–50.
- Herman, F., O. Beyssac, M. Brughelli, S. N. Lane, S. Leprince, T. Adatte, J. Y. Y. Lin, J.-P. Avouac, and S. C. Cox (2015), Erosion by an Alpine glacier, *Science*, *350*(6257), 193–195, doi:10.1126/science.aab2386.
- Hooke, R. L. B. (1984), On the role of mechanical energy in maintaining subglacial water conduits at atmospheric pressure, *J. Glaciol.*, *30*(105), 180–187.
- Hooke, R. L., S. B. Miller, and J. Kohler (1988), Character of the englacial and sub-glacial drainage system in the upper part of the ablation area of Storglaciären, Sweden, *J. Glaciol.*, *34*(117), 228–231.
- Hubbard, B. P., M. J. Sharp, I. C. Willis, M. K. Nielsen, and C. C. Smart (1995), Borehole water-level variations and the structure of the subglacial hydrological system of Haut Glacier d'Arolla, Valais, Switzerland, *J. Glaciol.*, *41*(139), 572–583.
- Iken, A. (1981), The effect of the subglacial water pressure on the sliding velocity of a glacier in an idealized numerical model, *J. Glaciol.*, *27*(97), 407–421.
- Iken, A., and R. A. Bindschadler (1986), Combined measurements of subglacial water pressure and surface velocity of Findelengletscher, Switzerland: Conclusions about drainage system and sliding mechanism, *J. Glaciol.*, *32*(110), 101–119.
- Kamb, B. (1987), Glacier surge mechanism based on linked cavity configuration of the basal water conduit system, *J. Geophys. Res.*, *92*(B9), 9083–9100, doi:10.1029/JB092iB09p09083.
- Kamb, B., C. F. Raymond, W. D. Harrison, H. Engelhardt, K. A. Echelmeyer, N. Humphrey, M. M. Brugman, and T. Pfeffer (1985), Glacier surge mechanism: 1982–1983 Surge of Variegated Glacier, Alaska, *Science*, *227*(4686), 469–479, doi:10.1126/science.227.4686.469.
- Kohler, J. (1995), Determining the extent of pressurized flow beneath Storglaciären, Sweden, using results of tracer experiments and measurements of input and output discharge, *J. Glaciol.*, *41*(138), 217–231.
- Legchenko, A., et al. (2014), Monitoring water accumulation in a glacier using magnetic resonance imaging, *Cryosphere*, *8*(1), 155–166, doi:10.5194/tc-8-155-2014.

- Lliboutry, L. (1968), General theory of subglacial cavitation and sliding of temperate glaciers, *J. Glaciol.*, *7*, 21–58.
- Lliboutry, L. (1983), Modifications to the theory of intraglacial waterways for the case of subglacial ones, *J. Glaciol.*, *29*(101), 216–226.
- Mair, D., P. Nienow, M. Sharp, T. Wohlleben, and I. Willis (2002), Influence of subglacial drainage system evolution on glacier surface motion: Haut Glacier d'Arolla, Switzerland, *J. Geophys. Res.*, *107*(B8), 2175, doi:10.1029/2001JB000514.
- Manning, R. (1891), On the flow of water in open channels and pipes, *Trans. Inst. Civ. Eng.*, *20*, 161–207.
- Mathews, W. H. (1964), Water pressure under a glacier, *J. Glaciol.*, *5*(38), 235–240.
- Motyka, R. J., S. O'Neel, C. L. Connor, and K. A. Echelmeyer (2003), Twentieth century thinning of Mendenhall Glacier, Alaska, and its relationship to climate, lake calving, and glacier run-off, *Global Planet. Change*, *35*(1–2), 93–112, doi:10.1016/S0921-8181(02)00138-8.
- Murray, T., and G. K. C. Clarke (1995), Black-box modeling of the subglacial water system, *J. Geophys. Res.*, *100*(B6), 10,231–10,245, doi:10.1029/95JB00671.
- Nye, J. F. (1976), Water flow in glaciers: Jökulhlaups, tunnels and veins, *J. Glaciol.*, *17*, 181–207.
- Riihimäki, C. A., K. R. MacGregor, R. S. Anderson, S. P. Anderson, and M. G. Liso (2005), Sediment evacuation and glacial erosion rates at a small alpine glacier, *J. Geophys. Res.*, *110*, F03003, doi:10.1029/2004JF000189.
- Röthlisberger, H. (1972), Water pressure in intra- and subglacial channels, *J. Glaciol.*, *11*(62), 177–203.
- Schmandt, B., R. C. Aster, D. Scherler, V. C. Tsai, and K. Karlstrom (2013), Multiple fluvial processes detected by riverside seismic and infrasound monitoring of a controlled flood in the Grand Canyon, *Geophys. Res. Lett.*, *40*, 4858–4863, doi:10.1002/grl.50953.
- Schoof, C. (2010), Ice-sheet acceleration driven by melt supply variability, *Nature*, *468*(7325), 803–806, doi:10.1038/nature09618.
- Schoof, C., C. A. Rada, N. J. Wilson, G. E. Flowers, and M. Haseloff (2014), Oscillatory subglacial drainage in the absence of surface melt, *Cryosphere*, *8*(3), 959–976, doi:10.5194/tc-8-959-2014.
- Stenborg, T. (1969), Studies of the internal drainage of glaciers, *Geogr. Annaler.*, *51A*, 13–41, doi:10.2307/520550.
- Strickler, A. (1923), Beiträge zur Frage der Geschwindigkeitsformel und der Rauheitszahlen für Ströme, Kanäle und geschlossene Leitungen, *Tech. Rep. 16*, Mitteilungen des Eidgenössischen Amtes für Wasserwirtschaft, Bern.
- Strickler, A. (1981), Contributions to the question of a velocity formula and roughness data for streams, channels and closed pipelines, Rep. T - 10, Translated from German by T. Roesgen et al., Lab. of Hydraul. and Water Resour., Calif. Inst. of Technol., Pasadena.
- Tsai, V. C., B. Minchew, M. P. Lamb, and J.-P. Ampuero (2012), A physical model for seismic noise generation from sediment transport in rivers, *Geophys. Res. Lett.*, *39*, L02404, doi:10.1029/2011GL050255.
- Vincent, C., M. Desclotres, S. Garambois, A. Legchenko, H. Guyard, and A. Gilbert (2012), Detection of a subglacial lake in Glacier de Tête Rousse (Mont Blanc area, France), *J. Glaciol.*, *58*(211), 866–878, doi:10.3189/2012JoG11J179.
- Werder, M. A., I. J. Hewitt, C. G. Schoof, and G. E. Flowers (2013), Modeling channelized and distributed subglacial drainage in two dimensions, *J. Geophys. Res. Earth Surf.*, *118*, 2140–2158, doi:10.1002/jgrf.20146.